

# Electron Backscatter Diffraction Analysis of effect of temperature on grain size, grain boundaries and texture of Aluminium Alloy 1050-H4 during Accumulative Roll Bonding Process (ARB)

M. Pita<sup>1,\*</sup>, P.M. Mashinini<sup>2</sup>, L.K. Tartibu<sup>2</sup>

<sup>1</sup>Department of Mechanical Engineering,  
Faculty of Engineering and Technology, University of South Africa

<sup>2</sup>Department of Mechanical and Industrial Engineering Technology,  
Faculty of Engineering and the Built Environment, University of Johannesburg

\*<sup>1</sup>[pitam@unisa.ac.za](mailto:pitam@unisa.ac.za), <sup>2</sup>[mmashinini@uj.ac.za](mailto:mmashinini@uj.ac.za), <sup>2</sup>[ltartibu@uj.ac.za](mailto:ltartibu@uj.ac.za)

## Abstract

This paper presents an Electron Backscatter Diffraction (EBSD) analysis of the effect of temperature on grain size, grain boundaries and texture of Aluminium Alloy 1050-H4 during Accumulative Roll Bonding (ARB). Two ARB cycles were performed in this study, at room temperature, and the samples were characterised by EBSD. The results show smaller grains after the 1<sup>st</sup> ARB pass, with substantial growth after the 2<sup>nd</sup> ARB pass due to the higher temperature owing to adiabatic warming. Noticeable fractions of equiaxed grains surrounded by low angle boundaries (misorientation <math>< 10^\circ</math>) are present in the microstructure of the sample after the 1<sup>st</sup> pass. 360 grains have a length of between 2 and 5  $\mu\text{m}$  after the 1<sup>st</sup> ARB pass, and the longest grains are between 68 and 72  $\mu\text{m}$ , which shows a significant decrease in size as compared to the sample before the ARB process. The sample after the 2<sup>nd</sup> ARB pass reveals that 147 grains have a length of between 2 and 8  $\mu\text{m}$  and the longest grains are between 131 and 137  $\mu\text{m}$ , which shows that the material experienced grain growth at this pass when compared to the grain size of the sample after the 1<sup>st</sup> ARB pass. Grain Misorientation distribution shows that the sample after the 1<sup>st</sup> ARB pass exhibits a higher frequency of low angle boundaries (<math>< 1.5^\circ</math>). It was observed that, after the 1<sup>st</sup> ARB pass where there is a significant decrease in grain size and more refined grains, the results also show strong fibre texture on X direction and Z plane at <math>\langle 100 \rangle</math> and <math>\langle 111 \rangle</math> respectively.

**Keywords:** grain size, EBSD, grain growth, temperature and ARB pass.

## 1. INTRODUCTION:

The concept of nanotechnology first appeared in a popular talk given by the physicist Feynman [1]. A major challenge remains the statistically relevant crystal structure and composition detection of nanocrystalline characteristics such as nanoparticles/nanoprecipitates in chemistry and alloy design using electron microscopy [2]. New techniques have been developed that include qualitative and quantitative 2D and 3D

microstructural data of high resolution (few 10s of nm) [3]. Among these are computer-integrated polarisation microscopy (CIP), electron backscatter diffraction (EBSD), serial sectioning in the SEM, and synchrotron X-Ray tomography using a focused-ion-beam (FIB) device [3]. EBSD – or Electron backscatter pattern (EBSP) – is a powerful tool that captures patterns of electron diffraction from crystals, which are components of material diffraction [4]. Captured patterns can then be used to evaluate the materials' crystallographic orientation or texture, which is closely linked to both material properties and efficiency [4]. EBSD is an effective material science tool and was used in the 1990s in the field of geology [5].

The good spatial resolution makes the inspection of grains of less than 1  $\mu\text{m}$  in size possible [6]. Representative microstructure maps are reconstructed to describe microstructure from the study of EBSD patterns [7]. Placing an appropriate area on the sample for collecting EBSD data is one challenge for EBSD work. It is difficult to imagine the sample surface with conventional secondary electron imaging (SEI) or backscattered electron imaging (BEI) as a highly tilted sample ( $70^\circ$ ) with a smooth surface is favoured for producing good EBSD patterns [8]. EBSD detectors also have diodes positioned at different locations around the perimeter of the phosphor panel to mitigate this difficulty [8]. Standard metallographic sectioning, grinding and polishing processes for EBSD are the starting point, but special care must be taken to ensure that the final polishing steps leave the sample surface free of any damage to the section, as the EBSD pattern is created from a very thin material surface layer (~40 nm) [9].

In recent years, severe plastic deformation (SPD) has been increasingly used in the processing of ultrafine grain (UFG, grain size in the 100-1000 nm range) or nanostructured (100 nm) materials directly from bulk samples such as equal channel angular pressing (ECAP), high-pressure torsion (HPT), cyclic extrusion compression (CEC) and accumulative roll bonding (ARB) [10]. The ultrafine grain (UFG) structure is supposed to result in higher strength, according to the Hall-Petch

relationship [11]. In economic terms, it is very important to produce high-strength materials, particularly without alloys [11]. UFG materials are typically stronger than traditional materials, which have grain sizes greater than a few tens of micrometres [12]. Saito et al. (1998) initially proposed the accumulative roll bonding (ARB) method to manufacture ultrafine-grained bulk aluminium sheets [13]. One of the most known processes for producing composite sheets from metallic sheets and for producing clad sheets is roll bonding [14]. Due to its viability as a continuous process, ARB has the potential to be adopted by industry to manufacture fine-grained materials in the form of large sheets [15]. Due to the repetitive cycles of cutting, piling, and roll bonding, the evolution of texture and microstructure in materials processed by accumulative roll-bonding (ARB) is complex [16].

EBSDB studies related to microstructure evolution, properties and texture of various materials have been conducted by several researchers. Tolaminejad et. al have studied microstructure evolution in a commercially pure aluminium severely deformed by Equal channel angular pressing (ECAP) using EBSD. Scanning revealed a homogeneous ultrafine-grained microstructure after 8 passes. This analysis also showed that the fraction of high angle grain boundaries and average grain size were about 70 % and 1500 nm, respectively [17]. As regards the application of the EBSD technique to ultrafine-grained and nanostructured materials processed by severe plastic deformation: Sample preparation, parameters optimisation and analysis were conducted by Chen et. al. in 2012. It was found that ion milling is a real universal and promising polishing method for EBSD preparation of almost all materials. There exists a maximum value of indexed points as a function of step size [10]. In 2018, Yvell et. al. used EBSD to analyse the surface and bulk microstructure evolution during interrupted tensile testing of a Fe - 19Cr - 12Ni alloy. The results show that the evolution of the deformation structure in surface and bulk grains displays a strong resemblance, but the strain needed to obtain a similar deformation structure is lower in the case of surface grains. The low SFE favours formation of deformation twins which reduces the slip distance, leading to a hardening like the Hall-Petch relation [18].

Electron backscatter diffraction (EBSD) is performed with the scanning electron microscope (SEM) to provide a wide range of analytical data, such as crystallographic orientation studies, phase identification and measurement of grain size [19]. The first step in data collection is the preparation of the specimen so that high-quality electron backscatter diffraction patterns (EBSD) can be observed and collected with the imaging system [20]. In general, almost all samples for EBSD observation need to be mechanically polished carefully [10]. Sample preparation include sectioning, mounting, grinding, polishing, colloidal silica, eletropolish, chemical etch, ion etch and conductive coating. In grain boundary colour map different colours are assigned to different ranges of grain boundary misorientation, shown as inset in the bottom-right corner of the image [4]. Grain boundaries with misorientation larger than 15 degree are considered high angle grain boundaries (HAGB) and are characterized as highly mobile grain boundaries [4]. The sizes and shapes of grains or subgrains in an EBSD map may be obtained by either linear intercept or grain reconstruction

methods [21]. When the orientation of grains is not random, the materials are textured. In order to describe texture one must determine how grains in a polycrystalline specimen are oriented in respect to the sample reference frame [22].

Aluminium alloys have been commonly used in the automotive industry in recent years. In particular, this is due to the real need to save weight to further minimise fuel consumption and exhaust emissions [23]. All the grain boundaries must be detected to accurately measure grain size. A primary parameter affecting a material property is grain size. Based on the literature survey, it could be observed that temperature increase during ARB leads to grain growth that negatively affects the properties of materials (mechanical properties) [24]. Due to the rise in grain curvature, from greater curvature to lower curvature, the rise in temperature leads to grain growth. This often contributes to the coalescence of grain and migration of grain, frequently resulting in the growth of grain. Instead of becoming smaller, the refined grain size that enhances material properties begins to develop [25].

Several methods have recently been used to stop these grain growth phenomena due to temperature changes, such as the use of solute additives that have a significant restriction due to foreign impurities in these additives that damage the material property [26]. Therefore, the use of an additive to prevent grain growth is not efficient in material science. It is better to design a material to be temperature sensitive and dependent without using additives and therefore it is important to study the critical temperature when grain growth start occurring during grain refinement by ARB.

Therefore, in the current study, the critical temperature when grain growth starts occurring, as well as the effects of surface temperature on grain size, grain boundaries and texture of AL-1050-H4 after the ARB process, will be investigated in order to design a material with stable and enhanced mechanical properties to be manufactured using ARB.

## 2. METHODOLOGY

### 2.1 ARB Experimentation

For this experiment, two roller rolling machines with rollers of 60 mm in diameters and 425 mm in length was employed. Motor speed was 1450 rpm, while gearbox input speed was 457.4 rpm and gearbox output speed p rpm. Because the roller shaft is coupled to the gearbox output shaft, the roller speed was also 9 rpm. The rolling machine concerned was located at the University of South Africa's laboratory. The material used was aluminium (Al 1050-H4), with dimensions of 2465mm x 25mm x 1.6mm. The rollers were aligned using a feeler gauge to ensure that the gap would be consistent across the rollers. The material was placed between the rollers and rolled at a pressure of 3.5 tons. For the first pass, the samples were pushed through the rollers during the deformation process. The two horizontal shafts took hold of the specimen and pushed it through the rollers. The thickness before and after the pass was measured using a micrometer. The material surface temperature was measured and recorded both before and after rolling using an infrared thermometer. The deformed material was then cut into two strips and the surfaces of each strip were cleaned in their

**Table 1:** Chemical composition of AL- 1050-H4 Alloy.

Cast No.	Alloy	O (%)	Fe (%)	Si (%)	Ag L	Al (%)
18122A44	1050	2.66+/-0.11	0.47+/-0.07	10.27+/-0.11	1.06+/-0.14	85.54+/-0.20

entirety with a wire brush, stacked together with bonding wire at the ends to ensure proper bonding and rolled again. This process was repeated twice. Three spot checks for chemical composition were performed on the parent sample using a Scanning Electron Microscope (SEM) and an Energy Dispersive X-ray (EDX) spectrometer to obtain the chemical composition of aluminium 1050-H4. The average values are presented in Table 1. The sample was prepared before analysis by SEM and EDX spectrometer. The specimen was placed inside the holder and fixed inside the instrument at a working distance of 10 mm. Voltage was 30 kV, with a 100x magnification value and 50 spot size. The average surface temperatures measured during the ARB process are presented in Table 2.

**Table 2:** Number of passes and temperatures

Number of passes	Surface temperature (0C)
Parent sample	24.1+/-0.01
1	27.2+/-0.1
2	29.5+/-0.11

## 2.2. EBSD Sample preparation and observation

Samples were cut, hot mounted in Bakelite on a citopress-10 at the rolling direction (RD). An all-purpose, Imperial Cloth has been selected for this work. 1.0 micron and 0.3-micron sizes of alumina suspensions were used. 39 N force was used, and the wheel was rotated at 130 rpm for 10 minutes for every abrasive size. Water was used as a lubricant. Samples were placed on a vibratory polisher for final polishing, a method by which the samples are subjected to low force and are pushed continuously over the polishing cloth by the vibratory movement. The all-purpose cloth was used again, but the final polishing medium was colloidal silica (CS) of 0.05 microns. Using the EBSD data acquisition and analysis software ATLAS, the EBSD patterns were obtained on a Zeiss Crossbeam 540 with 25kv and 10Na.

The area scanned was 1000 x 117  $\mu\text{m}$  x 87.3  $\mu\text{m}$ , with a step size of 0.46 micron and 200 x 584  $\mu\text{m}$  x 438  $\mu\text{m}$  with a step size of 2.3 microns. The working distance was 12-15 mm (typical for mounted samples in our SEM). One sample was analysed from each of the ARB samples and the parent sample. Three random areas were measured per sample. In HKL, Tango and Aztec used extrapolation to replace Zero indexed points and remove wild spikes. The samples showed a mean grain area of 10 pixels. Grains that touched the boundaries were removed. A standard 10-degree critical grain boundaries misorientation was used. Grain boundary length was determined by the longest linear dimension of the grain calculated from the maximum Ferret diameter ( $\mu\text{m}$ ). For the breadth, the shortest linear dimension of the grain was calculated from the minimum Ferret diameter ( $\mu\text{m}$ ).

Grain maps, grain size, grain misorientation distribution and texture were detected, captured and studied. Grain size measurements are presented in Table 3.

**Table 3:** Mean grain size measurements of the sample before and after the ARB process measured by EBSD.

Sample	Area ( $\mu\text{m}^2$ )	Breadth ( $\mu\text{m}$ )	Length ( $\mu\text{m}$ )	Surface temperature $^{\circ}\text{C}$
0 (parent sample)	108.20	10.77	16.90	24.1
1	16.83	3.17	5.21	27.2
2	55.39	3.84	6.58	29.5

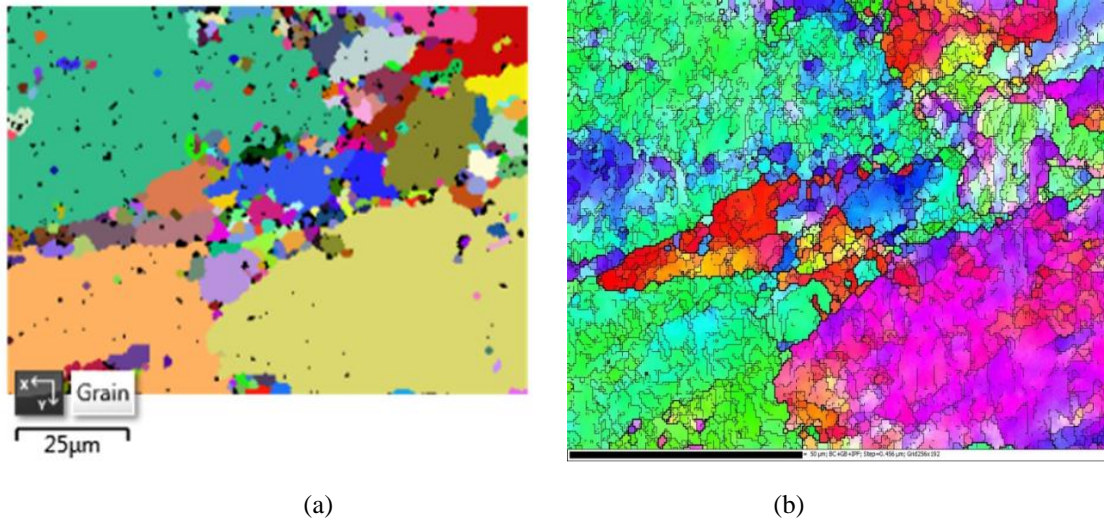
## 3. RESULTS AND DISCUSSION

### 3.1 Grain mapping

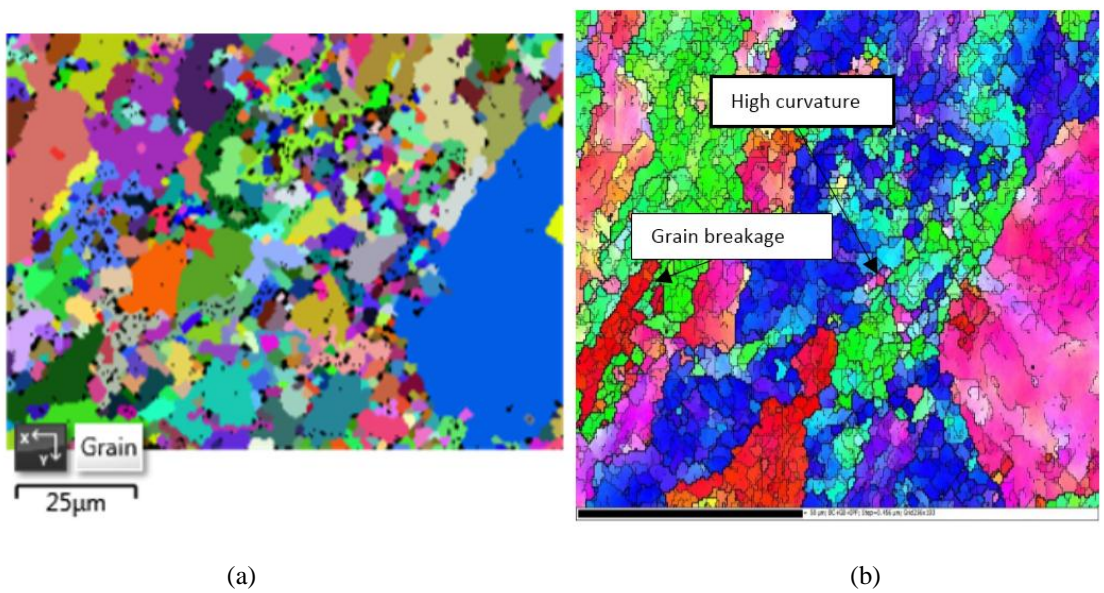
The three different samples discussed in the previous section were also analysed using the EBSD maps of the microstructure of AL 1050-H4 alloy. Grains were detected using a grain detection angle of 10 degrees and a minimum of 10 pixels within a grain. The results revealed in Figure 1(a-b) to 3(a-b) show different grain evolution during grain refinement. It is generally observed that the microstructure with laminar grains is revealed during deformation by ARB. The laminar grains are more visible in Figure 2(a-b) and 3(a-b) due to high pressure during grain refinement. It is also observed that increased lengthening due to high torsional stress during ARB leads to grain breakages and grain coalescence processes. As the grain becomes very small, the material experiences high vibrational stress and atomic mobility increases [27]. The high vibrational stress and mobility of atoms at nanoscales are easily affected by temperature, leading to grain growths as observed in Figure 3(a-b).

Figure 2(a-b) shows smaller grains that have grown substantially in Figure 3(a-b) due to higher temperatures arising from adiabatic warming. During such a warming process, conduction takes place. This is very bad since property enhancement then does not occur. A noticeable fraction of equiaxed grains surrounded by low angle boundaries (misorientation  $< 10^{\circ}$ ) are present in the microstructure of figure 2(a-b). Again, Figure 2(a-b) shows grains that are more stable since grain growth was not reported during grain refinement and therefore the operating temperature after the 1<sup>st</sup> pass was the critical operating temperature that enhanced material stability during grain refinement. The dislocation motion and grain boundaries migration have different curvatures due to adiabatic warming [28]. The curvatures in Figure 2(b) have higher curvature which enhances materials properties, while the curvature in Figure 3(b) revealed low

curvature with the result which does not enhance the material properties. The high and low grain curvatures are due to change in temperature, which enhanced properties. The grain sizes, as presented in Table 3, are discussed in the next section.



**Figure 1(a-b).** (a) Grain orientation map for parent sample and (b) Band contrast (BC) and Grain boundaries (GB) of parent sample.



**Figure 2(a-b).** (a) Grain orientation map of the sample after 1st of ARB pass and (b) BC and GB of the sample after 1st ARB pass.

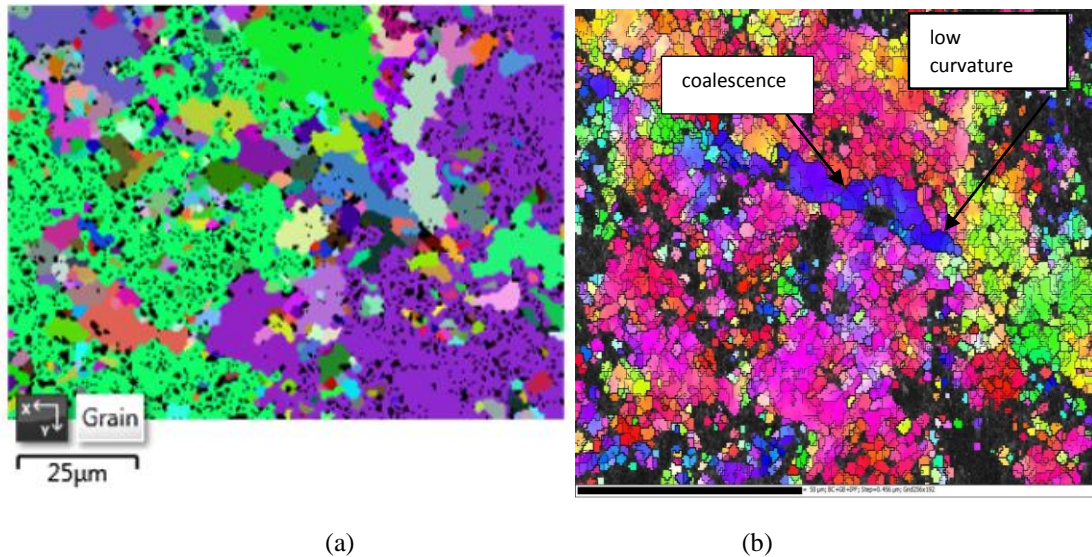


**Figure 3(a-b).** (a) Grain orientation map of the sample after 2nd pass of ARB pass and (b) BC and GB of the sample after 2nd ARB pass.

### 3.2 Grain size

As shown in Table 3, grains are detected with a mean grain area of  $108.20 \mu\text{m}^2$ , a mean breadth of  $10.77 \mu\text{m}$  and a mean length of  $16.90 \mu\text{m}$  at a room temperature of  $24.1^\circ\text{C}$ . After the 1st ARB pass, the grains were smaller as compared to the grain map of the sample before ARB process, which is presented in Table 3, and material surface temperature increased to  $27.4^\circ\text{C}$  due to friction between the material and rollers. This implies that there was a significant grain refinement that took place. Mean area was reported to be  $16.83 \mu\text{m}^2$ , mean breadth as  $3.17 \mu\text{m}$  and mean length as  $5.21 \mu\text{m}$ . It was observed that grain reduction was more than 60%. This shows that mechanical properties are enhanced at this stage. Similar findings have been reported by Tian et.al. (2019) in their study related to the geometrical potential and nanofiber membrane's highly selective adsorption property. Material can be strengthened by decreasing the average crystallite (grain) size. This size effect was found by Hall (1951) and Petch (1953) and the Hall–Petch relationship is now widely accepted for various applications [29].

Grains started to increase in size after the 2nd ARB pass. This was the result of the continued increase in the surface temperature of aluminium sample, which was reported to be  $29.5^\circ\text{C}$ . In a study of the theoretical model of nanomaterial heat content during grain refinement by accumulative roll bonding by Pita et. al., it was found that particle growths are reported at a very early stage in AL1050-H4 material when compared to other nanocrystalline materials [30]. The mean grain area at this stage (2<sup>nd</sup> ARB pass) was reported to be  $55.39 \mu\text{m}^2$ , which is three times more than the mean area of the sample after the 1<sup>st</sup> ARB pass. Breadth and length were reported to be  $3.84 \mu\text{m}$  and  $6.58 \mu\text{m}$  respectively. It was observed that grain growth started early due to the continuous increase in surface temperature, material chemical composition and the high amount of pressure applied, which was 3.5 ton on a thickness of 1.6mm.

### 3.3 Relationship between surface temperature and grain size

The results reflected in Table 3 are graphically demonstrated in Figure 4. It was observed that before the ARB process when the material surface temperature was  $24.1^\circ\text{C}$ , the grain breadth and length were  $10.77$  and  $16.90 \mu\text{m}$  respectively. The sample was rolled for the first pass and it was observed that the surface temperature increased to  $27.2^\circ\text{C}$ . In addition, it was also seen that there is a huge decrease in grain breadth and length, with these dimensions three times smaller than before the ARB process. This implies that the mechanical properties of the material were enhanced. The sample was rolled for the 2nd pass and it was noticed that the surface temperature continued to increase (due to friction) to  $29.5^\circ\text{C}$ . It was further observed that the grain breadth and length increased to  $3.84$  and  $6.58 \mu\text{m}$  respectively. Grain growth happened after the 2nd ARB pass, which is not good for material mechanical properties as it weakens the properties of the material. This is a similar result to that noted by Bhatt and Kholiya [24].

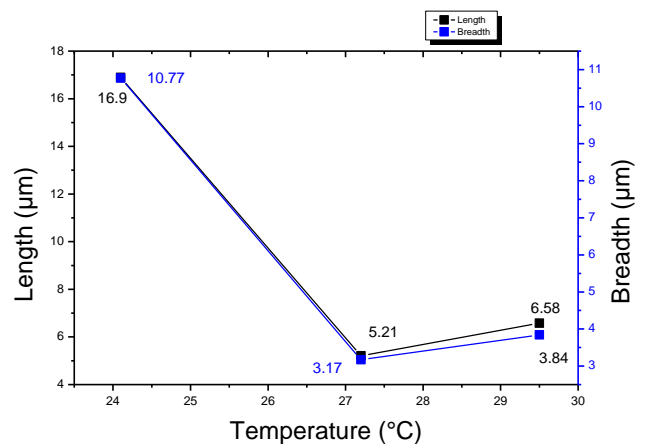


**Figure 4.** Graph of grain length and breadth against surface temperature.

It can be noted from Figure 5 that 110 grains of the sample before the ARB process had a length of between 10 and 16.8 $\mu\text{m}$ , which are shorter in this sample. From the same figure, it can be noted that there are about two longest grains, with a length of 55.6  $\mu\text{m}$ . Figure 6 shows that 360 grains have a length of between 2 and 5  $\mu\text{m}$ , which represents a significant decrease in size as compared to the sample before the ARB process. This implies that the mechanical properties of this material have been enhanced [31]. The results from the sample after the 2nd ARB pass, as presented in Figure 7, reveal that 147 grains have

a length of between 2 and 8  $\mu\text{m}$ , with the longest grains being between 131 and 137  $\mu\text{m}$ . These results show the increase in grain size as compared to the results of the sample after 1st ARB pass. The results also show that grain growth started after the 2nd ARB pass due to a continuous increase in surface temperature, as this sample has grains with bigger lengths as compared to the sample after 1<sup>st</sup> pass. Grain growth reduces material mechanical properties. After this pass, grains had high angle boundaries as compared to after the 1st ARB pass.

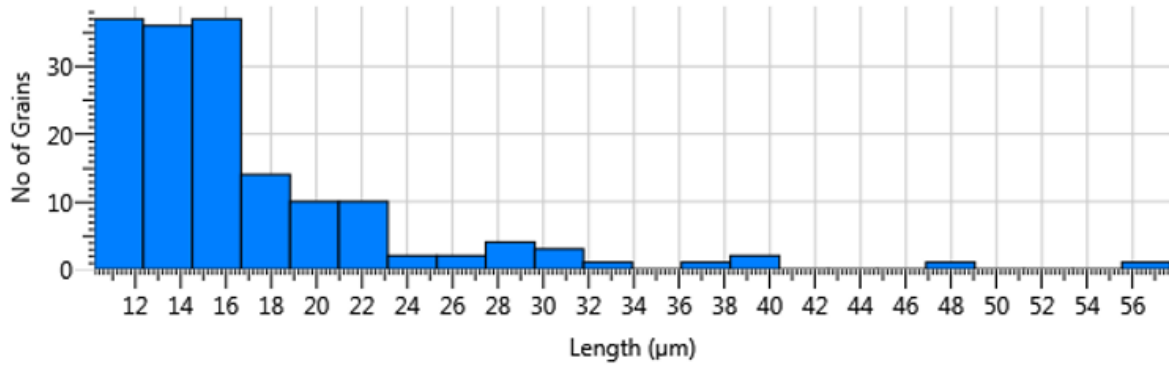


Figure 5. Graphical EBSD results samples before ARB.

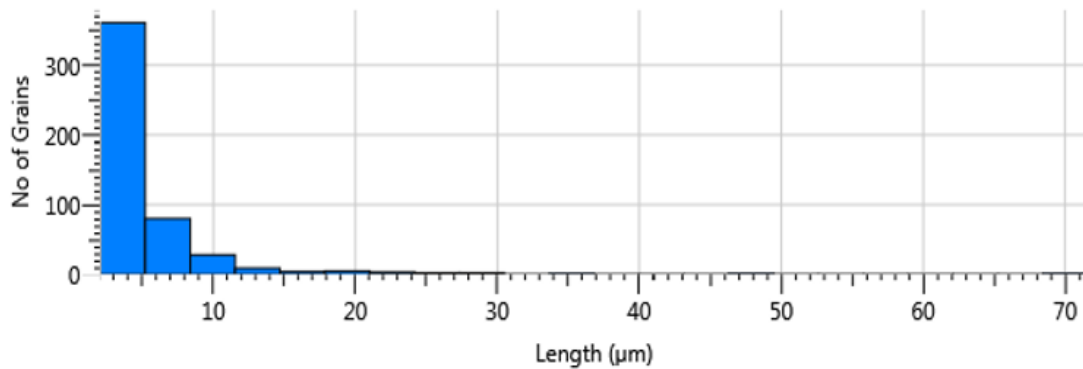


Figure 6. Graphical EBSD results of the sample after 1st ARB pass.

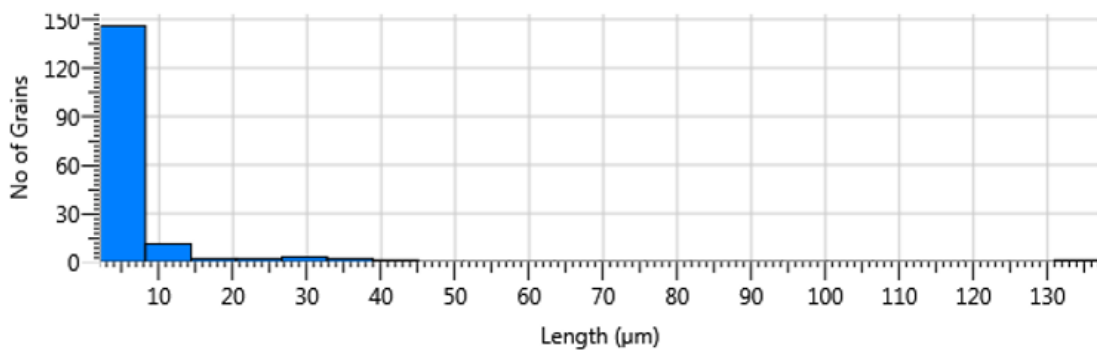


Figure 7. Graphical EBSD results of the sample after 2nd ARB pass

### 3.4 Grain misorientation distribution

Three samples characterized were of the same material (Al – 1050 – H4). The percentage refers (which is shown in figure 8 to 10) to the number of points that were positively identified for Al, only 70.2% of the total measured points were Aluminium, the rest which is 29.8% were not solved. These results come from the un-rolled sample. The other two samples which are samples after 1st and 2nd ARB pass had 100% solved phases.

Figures 8 to 10 show histograms of the grain boundary of the parent sample, of the sample after the 1st ARB pass and of the sample after the 2nd ARB pass. The tested samples differ in

grain boundary misorientation. The parent sample, which is the sample before the ARB process, is dominated by a higher frequency of angle boundaries between 0.1-3.5°. Figure 9 shows that grains exhibit a higher frequency of low angle boundaries (<1.5°). This is an indication that the material is more stable at this pass and that mechanical properties are further enhanced at this stage. Figure 10 is characterised by a higher frequency of angles of more than 1.5° when compared to Figure 9. This occurs when the material starts to experience grain growth due to continued increases in surface temperature.

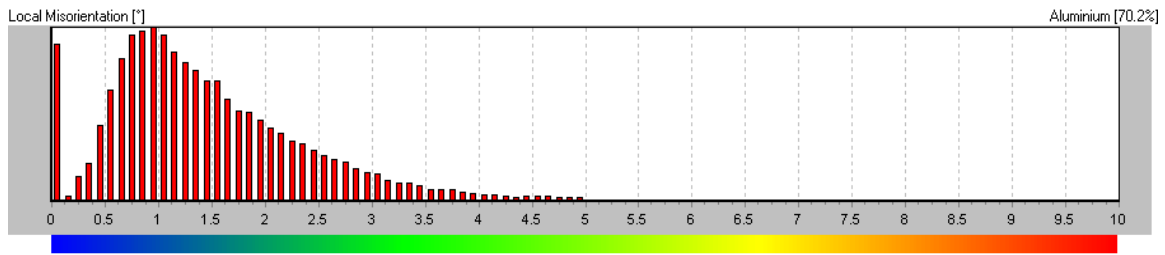


Figure 8. Histogram grain misorientation distribution of the parent sample.

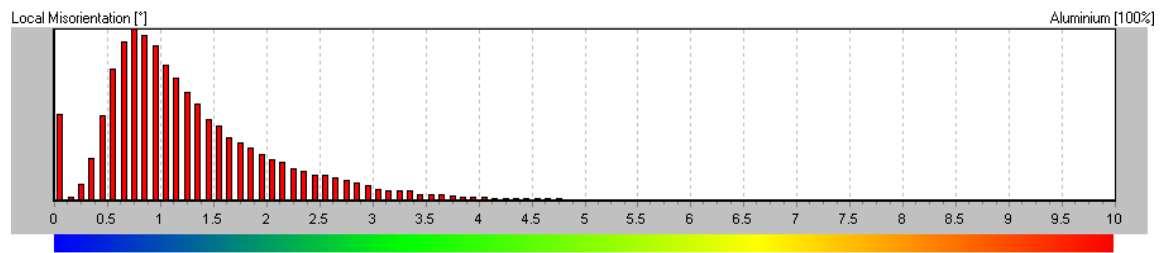


Figure 9. Histogram grain misorientation distribution of the sample after 1st ARB pass.

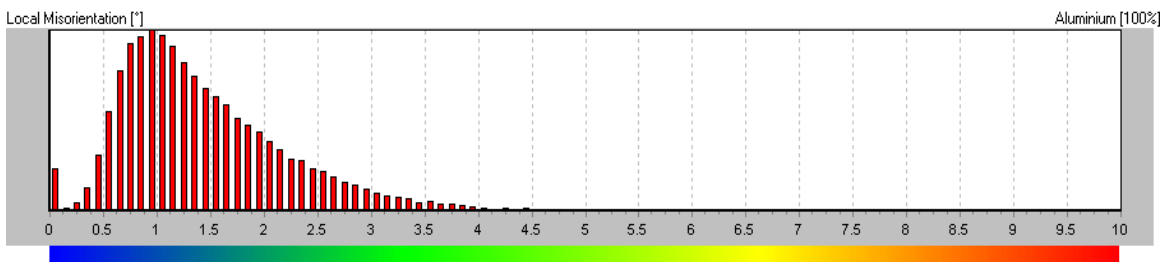


Figure 10. Histogram grain misorientation distribution of the sample after 2nd ARB pass.

### 3.5 ARB Samples Texture

The orientation distributions of grains of aluminium 1050-H4 alloy before and after an accumulative roll bonding process are presented from Figure 11 to Figure 13 by inverse pole figures on the X, Y and Z directions. From Figure 11, it can be noticed that the sample has a strong <110> fibre texture along the Y plane. This result was drawn from the original sample before the accumulative roll bonding process. It was observed that after the 1st ARB pass – where there is a significant decrease in grain size and more refined grains – the results show strong

<100> fibre texture on the X direction as well as strong <111> fibre texture on the Z plane. At this stage, the surface temperature was 27.2°C. After the 2nd ARB pass, the start of grain growth – caused by the continuous increase in surface temperature – was noticed. EBSD results in Figure 13 show the strong <111> fibre texture along the X plane and strong <100> fibre texture along the Y direction. This suggests that the texture during Severe Plastic Deformation (SPD) processing will most likely show [100]//ND, [111]//ND and [110]//RD components. The material properties of many important

engineering materials are strong [22].

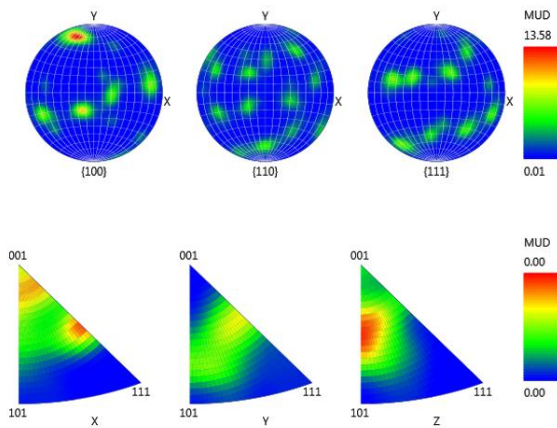


**Figure 11.** Representation of fibre textures by Miller indices showing inverse pole figures on X, Y and Z direction of the parent sample

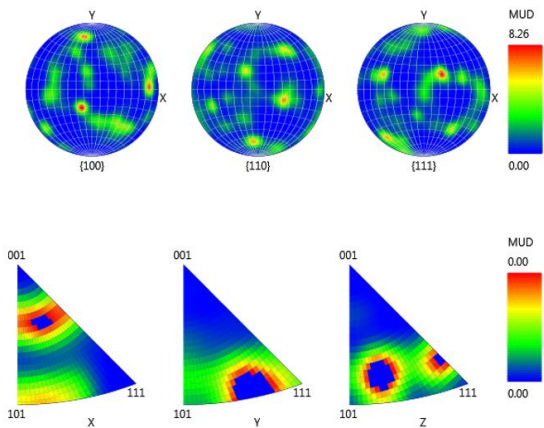


**Figure 12.** Representation of fibre textures by Miller indices showing inverse pole figures on X, Y and Z direction of the sample after 1st ARB pass.

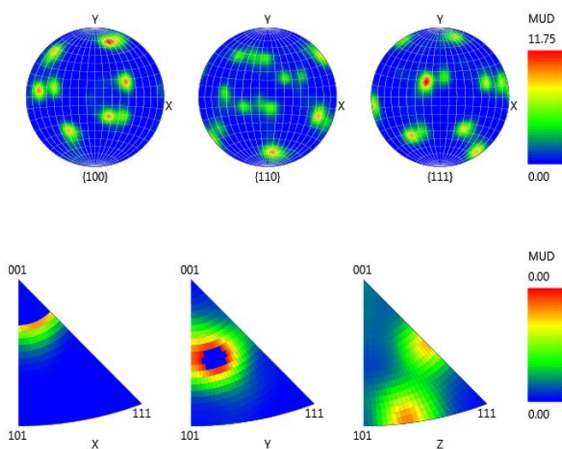


**Figure 13.** Representation of fibre textures by Miller indices showing inverse pole figures on X, Y and Z direction of the sample after 2nd ARB pass.

#### 4 CONCLUSION

The critical temperature at which grain growth starts to occur and the effect of temperature on grain size, grain boundaries and texture of AL-1050-H4 were investigated in this study. The ARB experiment was conducted at room temperature, at a constant speed and using constant force. The increase in material surface temperature during this process was due to friction between the rollers and the material being rolled. The EBSD analysis showed smaller grains that grew substantially due to the higher temperature as a result of adiabatic warming. Grain refinement was identified after the 1<sup>st</sup> ARB pass. As the grain became very small, the material experienced high vibrational stress and atomic mobility increased. This high vibrational stress and the mobility of atoms at nanoscales are easily affected by temperature (29.5°C), leading to grain growth as observed after the 2<sup>nd</sup> ARB pass. Grains were more stable after the 1<sup>st</sup> ARB pass since grain growth was not reported during grain refinement and therefore the operating temperature at this pass was the critical operation temperature that enhanced material stability during grain refinement. High and low curvature were noticed at the 1<sup>st</sup> and 2<sup>nd</sup> ARB passes respectively as a result of grain refinement and grain growth. Grain growth started early on this material – that is, after the 2<sup>nd</sup> ARB pass – due to a continuous increase in surface temperature. Strong fibre texture on the X and Z directions was observed at refined grains. The pattern of grain growth in nanomaterials due to adiabatic warming is a serious problem and needs to be addressed. The study managed to determine the critical temperature at which grain growth starts to occur on AL- 1050 – H4. It can be concluded that continuous increases in surface temperature result in grain growth and that this greatly affects the properties of the nanomaterials produced.

#### ACKNOWLEDGEMENTS

The research is supported by the University of Johannesburg and the University of South Africa.

#### REFERENCES

- [1] R. Kumar, G. Sharma, and M. Kumar, “Effect of size and shape on the vibrational and thermodynamic properties of nanomaterials,” *J. Thermodyn.*, vol. 1, no. 1, pp. 87–94, 2013.
- [2] A. Bhattacharya, C. M. Parish, J. Henry, and Y. Katoh, “High throughput crystal structure and composition mapping of crystalline nanoprecipitates in alloys by transmission Kikuchi diffraction and analytical electron microscopy,” *Ultramicroscopy*, vol. 202, no. March, pp. 33–43, 2019.
- [3] E. Mariani, “Electron backscatter diffraction (EBSD) in the SEM: applications to microstructures in minerals and rocks and recent technological advancements,” *Instrum. Tech. Appl. to Mineral. Geochemistry, Zaragoza*, vol. 120, no. 3, pp. 7–20, 2008.
- [4] D. Stojakovic, “Electron backscatter diffraction in materials characterization,” *Process. Appl. Ceram.*,

- vol. 6, no. 1, pp. 1–13, 2012.
- [5] S. Choi, S. Han, and Y. N. Lee, “Electron backscatter diffraction (EBSD) analysis of maniraptoran eggshells with important implications for microstructural and taphonomic interpretations,” *Palaeontology*, vol. 62, no. 5, pp. 777–803, 2019.
- [6] W. H. V. A. N. Geertruyden, S. R. Claves, and W. Z. Misiolek, “Electron Backscatter Diffraction Analysis of Microstructural Evolution in Hot-Deformed 6xxx Series Aluminum Alloys,” 2002.
- [7] V. S. Tong, A. J. Knowles, D. Dye, and T. Ben Britton, “Rapid electron backscatter diffraction mapping: Painting by numbers,” *Mater. Charact.*, vol. 147, pp. 271–279, 2019.
- [8] S. I. Wright, M. M. Nowell, R. De Kloe, P. Camus, and T. Rampton, “Electron imaging with an EBSD detector,” *Ultramicroscopy*, vol. 148, pp. 132–145, 2015.
- [9] A. J. Wilkinson and T. Ben Britton, “Strains, planes, and EBSD in materials science,” *Mater. Today*, vol. 15, no. 9, pp. 366–376, 2012.
- [10] Y. J. Chen, J. Hjelen, and H. J. Roven, “Application of EBSD technique to ultrafine grained and nanostructured materials processed by severe plastic deformation: Sample preparation, parameters optimization and analysis,” *Trans. Nonferrous Met. Soc. China (English Ed.)*, vol. 22, no. 8, pp. 1801–1809, 2012.
- [11] S. Tamimi, M. Ketabchi, N. Parvin, M. Sanjari, and A. Lopes, “Accumulative Roll Bonding of Pure Copper and IF Steel,” *Int. J. Met.*, vol. 2014, no. September, pp. 1–9, 2014.
- [12] A. Pramono, L. Kollo, and R. Veinthal, “Hot and cold regions during accumulative roll bonding of Al/Al<sub>2</sub>O<sub>3</sub> nanofibre composites,” *Proc. Est. Acad. Sci.*, vol. 65, no. 2, p. 132, 2016.
- [13] S. Sardar and A. Mandal, “Accumulative Roll Bonding of AA6005 and AA1060 Metal Strip : Study on Microstructure , Mechanical Properties and Evaluation of Minimum Bonding Criteria,” no. Aimtdr, pp. 1–6, 2014.
- [14] N. Nejad Fard, H. Mirzadeh, M. Rezayat, and J. Cabrera Marrero, “Accumulative Roll Bonding of Aluminum/Stainless Steel Sheets,” *J. Ultrafine Grained Nanostructured Mater.*, vol. 50, no. 1, pp. 1–5, 2017.
- [15] M. R. Rezaei, M. R. Toroghinejad, and F. Ashrafizadeh, “Production of nano-grained structure in 6061 aluminum alloy strip by accumulative roll bonding,” *Mater. Sci. Eng. A*, vol. 529, no. 1, pp. 442–446, 2011.
- [16] H. Wang, C. Lu, and K. Tieu, “A Combined Experiment and Crystal Plasticity FEM Study of Microstructure and Texture in Aluminium Processed by Reverse and Unidirectional Accumulative Roll-Bonding,” *Crystals*, vol. 9, no. 2, p. 119, 2019.
- [17] B. Tolaminejad, F. Brisset, and T. Baudin, “EBSD study of the microstructure evolution in a commercially pure aluminium severely deformed by ECAP,” *IOP Conf. Ser. Mater. Sci. Eng.*, vol. 32, no. 1, 2012.
- [18] K. Yvell, T. M. Grehk, P. Hedström, A. Borgenstam, and G. Engberg, “EBSD analysis of surface and bulk microstructure evolution during interrupted tensile testing of a Fe-19Cr-12Ni alloy Permanent link to this version : Materials Characterization EBSD analysi,” *Mater. Charact. J.*, vol. 141, pp. 8–18, 2018.
- [19] P. Voos, “Metallographic Preparation for Electron Backscattered Diffraction Patrick Voos Email : patrick.voos@buehler-met.de,” *Mater. Sci. Forum*, vol. 702–703, no. 2, pp. 2–5, 2011.
- [20] S. Tallur and S. A. Bhawe, “Specimen preparation for electron backscatter diffraction analysis,” 2012.
- [21] F. J. Humphreys, “Characterisation of fine-scale microstructures by electron backscatter diffraction (EBSD),” *Scr. Mater.*, vol. 51, no. 8 SPEC. ISS., pp. 771–776, 2004.
- [22] V. D. Cojocaru, D. Răducanu, I. Cinca, and A. Căprărescu, “Texture analysis by (110) pole figure for a SPD processed Ti-25Ta-25Nb alloy,” *UPB Sci. Bull. Ser. B Chem. Mater. Sci.*, vol. 74, no. 4, pp. 213–222, 2012.
- [23] I. M. Elseaidy, M. M. Ibrahim, M. M. Ghoneim, and M. E. A. EL-Azim, “Aluminum alloys strengthening by accumulative roll-bonding (arb) process,” *Trans. SMIRT*, pp. 1–10, 2007.
- [24] J. C. Bhatt and K. Kholiya, “Effect of size on the elastic and thermodynamic properties of nanomaterials,” *Indian J. Pure Appl. Phys.*, vol. 52, no. 9, pp. 604–608, 2014.
- [25] A. J. Haslam, D. Moldovan, S. R. R. Phillpot, D. Wolf, and H. Gleiter, “Combined atomistic and mesoscale simulation of grain growth in nanocrystalline thin films,” *Comput. Mater. Sci.*, vol. 23, no. 1–4, pp. 15–32, 2002.
- [26] H. Peng, Z. Jian, and F. Liu, “Review of thermo-kinetic correlation during grain growth in nanocrystalline materials,” *Int. J. Ceram. Eng. Sci.*, vol. 2, no. 2, pp. 49–65, 2020.
- [27] H. Zhou, H. Cui, and Q. H. Qin, “Influence of ultrasonic vibration on the plasticity of metals during compression process,” *J. Mater. Process. Technol.*, vol. 251, no. May 2018, pp. 146–159, 2018.
- [28] J. Favre *et al.*, “Modeling grain boundary motion and dynamic recrystallization in pure metals,” *Metall. Mater. Trans. A Phys. Metall. Mater. Sci.*, vol. 44, no. 13, pp. 5861–5875, 2013.
- [29] D. Tian, X. X. Li, and J. H. He, “Geometrical potential

and nanofiber membrane's highly selective adsorption property," *Adsorpt. Sci. Technol.*, vol. 37, no. 5–6, pp. 367–388, 2019.

- [30] M. Pita, M. P. Mashinini, and L. K. Tartibu, "Theoretical model of nanomaterial heat content (energy) during grain refinement by accumulative roll-bonding (ARB)," *Int. J. Eng. Res. Technol.*, vol. 13, no. 4, pp. 783–792, 2020.
- [31] M. Pita, P. M. Mashinini, and L. K. Tartibu, "Enhancing of aluminum alloy 1050-H4 tensile strength by accumulative roll bonding process," *Proc. 2020 IEEE 11th Int. Conf. Mech. Intell. Manuf. Technol. ICMIMT 2020*, vol. 13, pp. 31–35, 2020.